Activity-induced collapse and reexpansion of rigid polymers

J. Harder,[1] C. Valeriani,[2] and A. Cacciuto[1,*]

[1]*Department of Chemistry, Columbia University, 3000 Broadway, New York, New York 10027, USA*

[2]*Departamento de Quimica Fisica, Facultad de Ciencias Quimicas, Universidad Complutense de Madrid, 28040 Madrid, Spain*

(Received 9 October 2014; published 22 December 2014)

We study the elastic properties of a rigid filament in a bath of self-propelled particles. We find that while fully flexible filaments swell monotonically upon increasing the strength of the propelling force, rigid filaments soften for moderate activities, collapse into metastable hairpins for intermediate strengths, and eventually reexpand when the strength of the activity of the surrounding fluid is large. This collapse and reexpansion of the filament with the bath activity is reminiscent of the behavior observed in polyelectrolytes in the presence of different concentrations of multivalent salt.

DOI: 10.1103/PhysRevE.90.062312 PACS number(s): 83.80.Hj, 82.35.Lr, 82.20.Wt

I. INTRODUCTION

When a micron-sized object is immersed in a thermally equilibrated solution, it will undergo Brownian motion due to random collisions with the surrounding fluid. The situation is vastly different when this object is suspended in a bath of active (self-propelled) particles, especially when its shape is not spherical. Indeed, it is well known that self-propelled particles tend to accumulate around highly curved regions of suspended obstacles, thus generating local density gradients which can lead to effective propulsive forces, and anomalous rotational and translational diffusion. Recent work has explored the trapping of active particles on boundaries and microstructures of different shapes and how passive obstacles can become activated in the presence of an active bath [1–15]. More recently, we have explicitly characterized how the curvature of passive tracers is related to the extent of their activation [16]. Needless to say, having a way of selectively activating passive microstructures and their aggregates based on their shape is the first step towards the fabrication of microscopic engines, where the random active motion of one component can be converted into the persistent motion of another. A beautiful example of this process was recently shown in Refs. [17,18].

In this paper, we go one step further and consider the case of a passive structure with a flexible shape. Specifically, we study a semiflexible polymer (filament) confined in two dimensions in the presence of a low concentration of active spherical particles. Our analysis discusses the behavior of the filament for different values of the strength of the bath activity (characterized by the particles' self-propelling force) and of the filament rigidity. Recent work on active flexible filaments (i.e., chains formed by active Brownian particles) has shown very interesting phenomenological behavior, including periodic beating and rotational motion [19]. While preparing this manuscript, Kaiser *et al.* [20] have considered a system similar to ours, but in the fully flexible limit. In their study they show how a filament undergoes anomalous swelling upon increasing activity of the bath. Here, we confirm the results reported in Ref. [20], and show how adding rigidity to the filament leads to an even more complex nonmonotonic behavior, where the chain softens for moderate activities, can collapse into a metastable hairpin for intermediate activities, and behaves as a fully flexible chain in the large activity limit. Our data also indicate that at intermediate activities a rigid filament behaves as a two-state system that dynamically breathes between a tight hairpin and an ensemble of extended conformations.

II. METHODS

We perform numerical simulations of a self-avoiding polymer confined in a two-dimensional plane and immersed in a bath of spherical self-propelled particles of diameter σ, whose motion is described via the coupled Langevin equations

$$m\ddot{\boldsymbol{r}} = -\gamma\dot{\boldsymbol{r}} + F_a\boldsymbol{n}(\theta) - \partial_{\boldsymbol{r}}V + \sqrt{2\gamma^2 D}\boldsymbol{\xi}(t), \tag{1}$$

$$\dot{\theta} = \sqrt{2D_r}\xi_r(t). \tag{2}$$

Here, γ is the friction coefficient, V the pairwise interaction potential between the particles, and D and D_r are the translational and rotational diffusion constants, respectively, satisfying the relation $D_r = 3D/\sigma^2$. $\boldsymbol{n}(\theta)$ is a unit vector pointing along the propelling axis of the particles, and its orientation, tracked by the angular variable θ, is controlled by the simple rotational diffusion in Eq. (2). $F_a \geqslant 0$ is the magnitude of the self-propelling force acting on each particle. The solvent-induced Gaussian white-noise terms for both the translational and rotational motion are characterized by the usual relations $\langle\xi_i(t)\rangle = 0$, $\langle\xi_i(t)\cdot\xi_j(t')\rangle = \delta_{ij}\delta(t-t')$ and $\langle\xi_r(t)\rangle = 0$, $\langle\xi_r(t)\cdot\xi_r(t')\rangle = \delta(t-t')$. The polymer consists of $N = 70$ monomers of diameter σ, linearly connected via harmonic bonds according to the potential $U_b = \varepsilon_b(r-r_0)^2$, where r is the center-to-center distance between linked monomers, $\varepsilon_b = 10^3 k_B T/\sigma^2$, and $r_0 = 2^{1/6}\sigma$ is the equilibrium distance. An additional harmonic potential, $U_a = \kappa(\phi - \phi_0)^2$, is used to introduce angular rigidity to the polymer, where ϕ is the angle between adjacent bonds, and $\phi_0 = \pi$ is the equilibrium angle. Values of κ considered in this work range from 0 to $90k_BT$. The equation of motion of the filament monomers is given by Eq. (1), with $F_a = 0$.

The excluded volume between any two particles in the system (including the monomers in the chain) is enforced with

*ac2822@columbia.edu

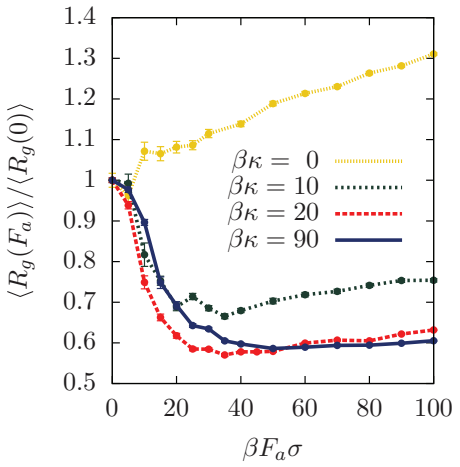

FIG. 1. (Color online) Time-averaged radius of gyration of a filament, normalized by its value calculated in the absence of activity ($F_a = 0$), as a function of the propelling force F_a for different filament rigidities, κ.

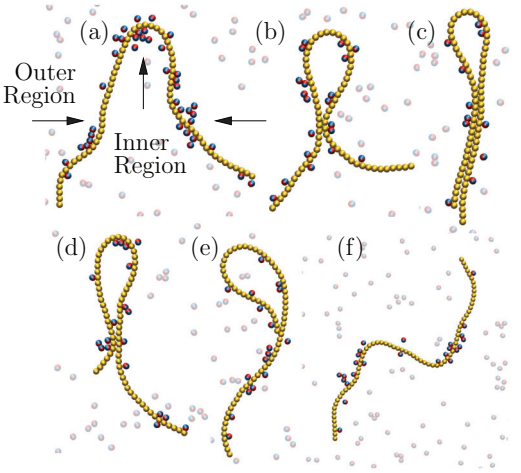

FIG. 2. (Color online) Snapshots from our simulations depicting the filament at various stages of folding and unfolding (a)→(f). The propelling force F_a acts along the axis connecting the poles of the two hemispheres we used to depict the active particles in the blue-to-red direction. Panel (a) shows explicitly our convention for the definition of inner and outer regions of a bent filament. For the sake of clarity, active particles away from the filament have been rendered with a semitransparent filter [26].

a purely repulsive Weeks-Chandler-Andersen potential

$$V(r) = 4\epsilon\left[\left(\frac{\sigma}{r}\right)^{12} - \left(\frac{\sigma}{r}\right)^{6} + \frac{1}{4}\right], \qquad (3)$$

with range extending up to $r = 2^{1/6}\sigma$. Here r is the center-to-center distance between any two particles, and $\varepsilon = 10k_{\mathrm{B}}T$. The simulation box is a square with periodic boundary conditions. All simulations have been performed using LAMMPS [21] at an active particle volume fraction $\phi = 0.1$ (corresponding to 318 active particles), which is sufficiently small to prevent spontaneous phase separation of the active particles [22,23]. Throughout this work we use the default dimensionless Lennard Jones units as defined in LAMMPS, for which the fundamental quantities mass m_0, length σ_0, epsilon ϵ_0, and the Boltzmann constant k_B are set to 1, and all of the specified masses, distances, and energies are multiples of these fundamental values. In our simulations we have $T = T_0 = \epsilon_0/k_B$, $m = m_0$, and $\sigma = \sigma_0$. Finally, $\gamma = 10\tau_0^{-1}$, where τ_0 is the dimensionless unit time defined as $\tau_0 = \sqrt{\frac{m_0\sigma_0^2}{\epsilon_0}}$.

III. RESULTS AND DISCUSSION

We begin our analysis by measuring the radius of gyration of the filament, $R_g^2 = \frac{1}{2N^2}\sum_{i,j}(\mathbf{r_i} - \mathbf{r_j})^2$, as a function of the strength of the propelling force of the surrounding particles in the bath, F_a, for different values of the chain angular rigidity κ. The results are shown in Fig. 1.

Consistent with the work by Kaiser *et al.* [20], a fully flexible self-avoiding filament swells when immersed in an active bath. This is due to the forces exerted on the filament by the active particles as they cluster along different regions of the filament and stretch it by pushing it in different directions. Interestingly, when the filament is somewhat rigid, the opposite behavior is observed. The radius of gyration decreases for small values of F_a, it reaches a minimum for intermediate activities, and it slowly begins to increase for large propelling forces. This nonmonotonic behavior of the radius of gyration with F_a is reminiscent of that of polyelectrolytes in the presence of multivalent salt [24] as a function of salt concentration.

When an active particle strikes a fully flexible filament, the filament can be stretched from a relatively compact configuration to a more extended one. However, when the filament is stiff, it is mostly stretched to begin with, and any local asymmetries in the number of active particles that cluster on either side of the filament can provide sufficiently large forces to bend it. As the filament begins to bend (say in the middle), different regions of its surface will have different exposure to the active particles. Specifically, the outer region [see Fig. 2(a)] will experience a larger number of collisions than the inner region as the former offers a larger cross section to the active particles. Simultaneously, active particles in the inner region tend to accumulate around the areas with highest curvature [15,16]. The combination of the forces acting on the inner and outer regions of the filament creates a pivot around which the filament can fold into a tight hairpin.

Because there are no direct attractive interactions between different parts of the filament or between the filament and the active particles, the hairpin eventually unfolds. This process is initiated by the active particles located in the inner region whose forces cause the location of the hairpin's head to slide along the filament, effectively shortening one arm and lengthening the other until full unfolding is achieved. Furthermore, fluctuations in the number of active particles applying a force on the outer arms of the filament allow it to open slightly, thus letting active particles either out of the inner region or into it. The first case stabilizes the hairpin structure whereas the second case de-stabilizes it. For a range of intermediate bath activities, the filament will therefore breath dynamically between a tightly folded and an ensemble of bent but extended configurations. Figure 2 shows several

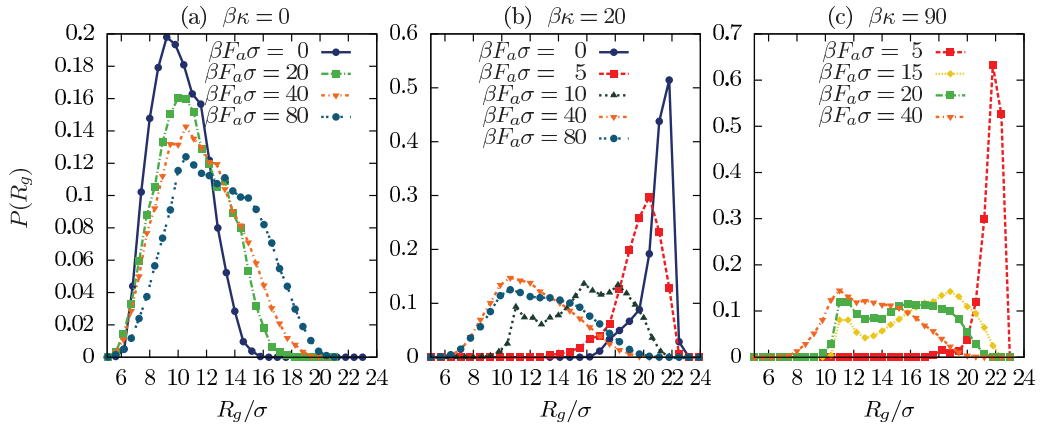

FIG. 3. (Color online) Probability distribution of the radius of gyration $P(R_g)$ for increasing values of the propelling forces F_a. Panel (a) shows the results for a fully flexible chain, panel (b) those for a polymer with rigidity $\beta\kappa = 20$, and panel (c) those for the stiffest polymer considered in this work, $\beta\kappa = 90$.

snapshots from our simulations highlighting the folding and unfolding of the filament.

It is worth mentioning how the position of the minimum in Fig. 1 shifts towards larger values of F_a upon increasing the rigidity of the polymer. This is not surprising as larger active forces are required to bend more rigid polymers. However, how exactly this minimum shifts is unclear because of the nontrivial dependence of the number of particles accumulating on the filament as a function of F_a. In general, an increase in F_a also comes with an increase in the average number of particles pushing on the filament, resulting in a net force which increases faster than linearly with F_a. This has been explicitly shown in our recent work [25] where we computed the force induced on two parallel rods by a bath of active spherical particles. The result is a complex dependence of the force between the rods on F_a, on the active particles density, and on the length on the rods which cannot be described with a single power law.

Given the complex dynamics observed in our simulations, the average value of the filament radius of gyration provides only a limited characterization of the system. Crucial information about the conformation of the filament can be extracted from the probability distribution, $P(R_g)$, of the radius of gyration, for different values of κ and F_a. For a fully flexible chain, Fig. 3(a), we observe that upon increasing the bath activity, the distribution, $P(R_g)$, begins to broaden towards larger values of R_g, indicating that the filament is able to reach configurations that are more extended (swollen) with respect to the typical behavior expected in the absence of active particles, which is consistent with recent results by Kaiser *et al.* For rigid filaments, Figs. 3(b) and 3(c), we observe the opposite behavior as a function of the bath activity. Namely, the sharply peaked distribution at large values of R_g that one would expect in the absence of particle activity and that corresponds to a fully stretched filament, broadens and shifts towards lower values of R_g as F_a is increased in the systems. This is indicative of the softening of the chain. Upon further increase of F_a, distinct peaks begin to develop (signature of the formation of folded conformations). Finally, for even larger values of F_a, we observe a broad distribution covering a wide range of R_g. Strikingly, the distributions in the large activity limit are independent of κ, suggesting that, as we will discuss later on, a rigid filament in a bath at large activity behaves akin to a fully flexible filament in the same bath.

Further evidence for the formation of hairpins and their relative stability with respect to more extended configurations can be obtained by combining calculations of R_g with the corresponding information about the asphericity of the filament. Following Rudnick *et al.* [27], we define asphericity as

$$\langle A \rangle = \frac{\sum_{i>j} \langle (\lambda_i - \lambda_j)^2 \rangle}{\left\langle \left(\sum_i \lambda_i \right)^2 \right\rangle}, \tag{4}$$

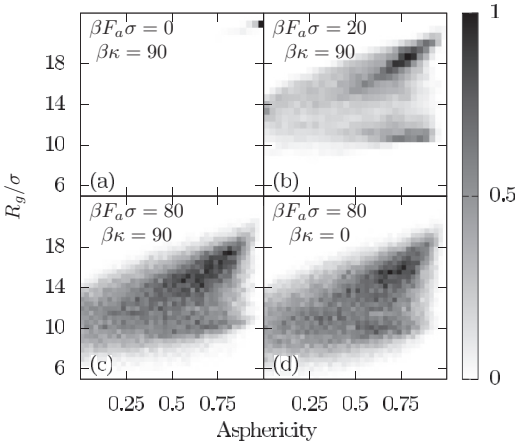

FIG. 4. Panels (a)–(c): Time-averaged probability distribution of finding a rigid filament, $\beta\kappa = 90$, with a given radius of gyration R_g and asphericity A for different values of F_a. When $\beta F_a\sigma = 0$, panel (a), the filament is almost exclusively extended ($A \sim 1$, $R_g \sim 22\sigma$). At $\beta F_a\sigma = 20$, panel (b), two distinct peaks can be seen at large values of the asphericity, where one has roughly half the R_g of a fully extended chain. These peaks correspond to the folded (hairpin) and unfolded (extended) states. At larger values of F_a, panel (c), the distribution smears out and the filament can more freely explore a wider variety of configurations. Note how the distribution in panel (c) is very similar to that in panel (d) corresponding to a fully flexible filament, $\beta\kappa = 0$, in an active fluid having the same propelling force $\beta F_a\sigma = 80$. All distributions have been divided by their respective maximum values so that they can be represented with the same color scale.

where λ_i is the ith eigenvalue of the shape tensor. In two dimensions, this parameter is equal to zero for a circular or isotropic object, and 1 for an object which extends along one dimension. In our system, small values represent configurations where the filament is relatively symmetric about its center of mass, whereas large values indicate a fully stretched, rigid filament.

We show the result of this analysis for $\beta\kappa = 90$ in Fig. 4, where we plot the time-averaged probability distribution of configurations with a given R_g and asphericity, A. When $\beta F_a\sigma = 0$ the plot shows, as expected, a distribution centered around large values of R_g and A close to 1, corresponding to a stiff filament. As the bath activity increases, at $\beta F_a\sigma = 20$ two distinct high probability regions emerge. Both have large asphericities, indicating elongated configurations, but with well separated values of R_g. The folded configuration has a value of $R_g \sim 11\sigma$ and the unfolded corresponds to $R_g \sim 18\sigma$. This scenario, consistent with our previous analysis, suggests a two-state system (folded-unfolded) where the two states have comparable probabilities. As F_a is further increased, the distribution smears out as local folding and unfolding of filament segments begins to occur at every length scale along the chain and the filament's statistics begin to resemble that of a fully flexible swollen polymer. For comparison we also show in the same figure (bottom right) the probability distribution for a fully flexible filament immersed in a bath with the same active force.

IV. CONCLUSIONS

In this paper we studied the behavior of a rigid filament immersed in a low volume fraction suspension of active particles confined in two dimensions as a function of filament rigidity and bath activity. Using shape-sensitive observables, we have characterized the conformational properties of the filament. Our findings indicate that fully flexible filaments swell monotonically with bath activity, but rigid filaments present a more peculiar nonmonotonic behavior. For small activities, rigid filaments soften and become more flexible. As the bath activity is further increased, we observe the formation of a two-state system characterized by extended and hairpin configurations, with complex local dynamics leading to their formation and destabilization. Finally, in the large bath activity limit the behavior of fully flexible and rigid filaments becomes nearly identical with a large distribution of accessible filament conformations. It should be stressed that this behavior is peculiar to two-dimensional or quasi-two-dimensional confinement. In fact, simulations of the same system in three dimensions (not presented) do not show traces of the remarkable phenomenology observed in two dimensions. This is because of the reduced probability of a collision between active particles and filaments, but more importantly because of the inability of a one-dimensional filament to effectively trap active particles in three dimensions. We however expect a behavior similar to that observed for polymers in two-dimensional membranes embedded in a three-dimensional bath of active particles. Work in these directions will be published elsewhere.

ACKNOWLEDGMENTS

A.C. acknowledges financial support from the National Science Foundation under Grant No. DMR-1408259. C.V. acknowledges financial support from a Juan de la Cierva Fellowship, from the European Marie Curie Integration Grant No. 322326-COSAAC-FP7-PEOPLE-CIG-2012, and from the Spanish National Project No. FIS2013-43209-P.

[1] J. Tailleur and M. E. Cates, Europhys. Lett. **86**, 60002 (2009).
[2] A. Morozov and D. Marenduzzo, Soft Matter **10**, 2748 (2014).
[3] A. Kaiser, A. Peshkov, A. Sokolov, B. ten Hagen, H. Löwen, and I. S. Aranson, Phys. Rev. Lett. **112**, 158101 (2014).
[4] M. B. Wan, C. J. Olson Reichhardt, Z. Nussinov, and C. Reichhardt, Phys. Rev. Lett. **101**, 018102 (2008).
[5] A. Kaiser, H. H. Wensink, and H. Löwen, Phys. Rev. Lett. **108**, 268307 (2012).
[6] A. Kaiser, K. Popowa, H. H. Wensink, and H. Löwen, Phys. Rev. E **88**, 022311 (2013).
[7] L. Angelani and R. Di Leonardo, New J. Phys. **12**, 113017 (2010).
[8] H. H. Wensink, V. Kantsler, R. E. Goldstein, and J. Dunkel, Phys. Rev. E **89**, 010302 (2014).
[9] X.-L. Wu and A. Libchaber, Phys. Rev. Lett. **84**, 3017 (2000).
[10] J. Elgeti and G. Gompper, Europhys. Lett. **101**, 48003 (2013).
[11] S. A. Mallory, A. Šarić, C. Valeriani, and A. Cacciuto, Phys. Rev. E **89**, 052303 (2014).
[12] H. H. Wensink and H. Löwen, Phys. Rev. E **78**, 031409 (2008).
[13] K. C. Leptos, J. S. Guasto, J. P. Gollub, A. I. Pesci, and R. E. Goldstein, Phys. Rev. Lett. **103**, 198103 (2009).
[14] D. Ray, C. Reichhardt, and C. J. Olson Reichhardt, Phys. Rev. E **90**, 013019 (2014).
[15] Y. Fily, A. Baskaran, and M. F. Hagan, Soft Matter **10**, 5609 (2014).
[16] S. A. Mallory, C. Valeriani, and A. Cacciuto, Phys. Rev. E **90**, 032309 (2014).
[17] L. Angelani, R. Di Leonardo, and G. Ruocco, Phys. Rev. Lett. **102**, 048104 (2009).
[18] R. Di Leonardo, L. Angelani, D. Dell'Arciprete, G. Ruocco, V. Iebba, S. Schippa, M. P. Conte, F. Mecarini, F. De Angelis, and E. Di Fabrizio, Proc. Natl. Acad. Sci. USA **107**, 9541 (2010).
[19] R. Chelakkot, A. Gopinath, L. Mahadevan, and M. Hagan, J. R. Soc. Interface **11**, 20130884 (2014).
[20] A. Kaiser and H. Löwen, J. Chem. Phys. **141**, 044903 (2014).
[21] S. Plimpton, J. Comput. Phys. **117**, 1 (1995).
[22] Y. Fily and M. C. Marchetti, Phys. Rev. Lett. **108**, 235702 (2012).
[23] J. Stenhammar, D. Marenduzzo, R. J. Allen, and M. E. Cates, Soft Matter **10**, 1489 (2014).
[24] P.-Y. Hsiao and E. Luijten, Phys. Rev. Lett. **97**, 148301 (2006).
[25] J. Harder, S. A. Mallory, C. Tung, C. Valeriani, and A. Cacciuto, J. Chem. Phys. **141**, 194901 (2014).
[26] W. Humphrey, A. Dalke, and K. Schulten, J. Mol. Graphics **14**, 33 (1996).
[27] J. Rudnick and G. Gaspari, J. Phys. A: Math. Gen. **19**, L191 (1986).